ACS OMEGA

Article

Cite This: ACS Omega 2019, 4, 16733−16742

http://pubs.acs.org/journal/acsodf

Nanonetwork of Coordination Polymer AHMT-Ag for the Effective and Broad Spectrum Detection of 6-Mercaptopurine in Urine and Blood Serum

Vinita,[†,§] Madhu Tiwari,[‡] Neha Agnihotri,[∥] Monika Singh,[†] Akhilesh Kumar Singh,[†] and Rajiv Prakash*[,†]

[†]School of Materials Science and Technology, Indian Institute of Technology (Banaras Hindu University), Varanasi 221005, India

[‡]Department of Chemistry, K. N. Govt. P. G. College Gyanpur, Bhadohi 221304, India

[§]Department of Chemistry, DDU Gorakhpur University, Gorakhpur 273009, India

[∥]Department of Physics, National Institute of Technology, Jamshedpur 832109, India

Supporting Information

ABSTRACT: Nanocrystalline coordination polymers (NCCPs) have been considered as an incredible electrochemical sensor for the effective detection of biologically dynamic drug 6-mercaptopurine (6-MP). In the present report, a significantly stable infinite arrayed coordination polymeric network was self-assembled via metal with efficient organic tecton 4-amino-3-hydrazino-5-mercapto-1,2,4,-triazole (AHMT) in which silver(I) ions are coordinated by AHMT via hydrazino and exocyclic thiol linkage to form AHMT-Ag NCCP. An efficient and highly sensitive detection of 6-MP is attained owing to eminent electron channeling via polymeric nanocrystallite pores. An effective charge transfer leads to an interface of the AHMT-Ag nano-pores and electrolyte anchored electrode via $\pi-\pi$ electron coupling and hydrophobic interaction. The voltammogram exposes acute redox behavior of 6-MP and discloses an impeccable illustration for the AHMT-Ag facilitated oxidation of 6-MP. This unique signature was applied in voltammetric detection of 6-MP in blood serum, human urine, and pharmaceutical formulation (tablet) by a considerable high sensitivity of 0.074, 0.058, and 0.036 μA/μM and a detection limit of 87, 97, and 37 nM, respectively. Thus, the prepared AHMT-Ag NCCP can provide a valuable platform for fabrication of highly sensitive electrochemical devices to assay biologically essential drug molecules.

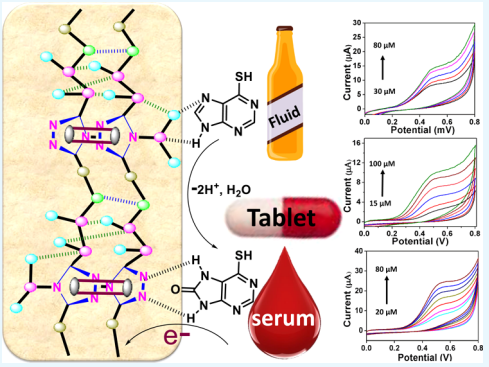

1. INTRODUCTION

Nanocrystalline coordination polymers-(NCCPs) are an attractive class of tailorable material and exhibit outstanding properties that expands the scope in various areas.[1] The significant research interest in the domain of these important scaffold are due to their specific size, structural regularity, high surface area, high porosity, design ability, and easy tunability results to a larger potential in different applications.[2−5] Nano size of these crystalline coordination polymeric regimes are of large significance in catalysis, thin film devices, and drug delivery.[6,7] Owing to these features recent research affords for the sketch of fashionable organization of metal ions with organic tecton results with a huge potential for various applications.[8−10] Geometry and coordination manner of organic tecton and metal center affects the properties and structure of NCCP, other secondary interactions, such as hydrogen bonding also results in the versatile properties of NCCPs.[11,12] In this regard, 4-amino-3-hydrazino-5-mercapto-1,2,4-triazole (AHMT), an efficient organic tecton used for the production of functional NCCP. Nitrogen and sulfur atoms facilitate coordination of organic tecton with a metal ion throughout the arrangement to create a functional structure. Because of structural tailorability of the organic tecton and capability to regulate the assembly with a metal ion at the nanoextent, they have fascinating applications in energy storage,[13] catalysis,[14] adsorption,[15] efficient contrast agents,[16] biotechnology,[17] nanofluids,[18] gas separation,[19] chemical sensing,[20,21] light harvesting,[22] device formation[23] and drug delivery,[24] selective catalysis,[25] fuel cells,[26] and so forth. The prominent interactions are metal−ligand interactions that create extra strong entities. Furthermore, the $\pi-\pi$ stacking between polymer chains that inter- and intra-hydrogen bonding direct toward an organization and definite alignment of these structures.[27]

In the view of the above particulars, our research interest is preparation of unique nanosized coordination polymers with reasonable organic building blocks and electrochemical sensing of frequently used drugs; here we first time explore the

Received: April 18, 2019
Accepted: September 11, 2019
Published: October 4, 2019

DOI: 10.1021/acsomega.9b01122
ACS Omega 2019, 4, 16733−16742

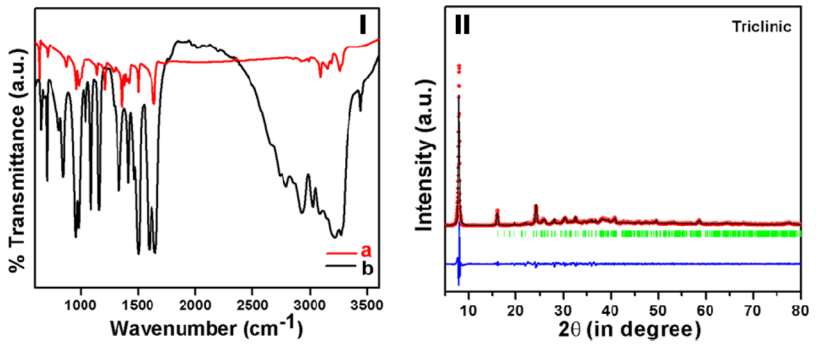

Figure 1. (I) FT-IR spectra (a) AHMT-Ag (b) AHMT and (II) Le-bail fit of AHMT-Ag.

development of AHMT-Ag NCCPs with an identical crystalline structure, high solvent dispersibility, and electrochemical activity for sensing application.

AHMT-Ag NCCP was formulated under optimal conditions at ambient temperature without any additional supplements. The optimization of reactant concentration is executed while synthesis and monitored by using appropriate characterization techniques. During synthesis the Ag(I) ions coordinate to nitrogen and sulfur atoms of the linker resulting in exceptional capability requisite for molecular amendment of the inner pore architecture. Thus, NCCPs cover huge advantages for the valuable application. This platform is advantageous for various sensing applications because of its multiple binding sites.

At present there is a number of lifesaving drugs frequently used every day, when their amount exceeds above a certain level it causes toxicity. 6-Meracaptopurine (6-MP), an excessively important immunosuppressive drug, is used in anticancer chemotherapy for dealing acute lymphoblastic leukemia and inflammatory bowel disease. Generally, the 6-MP concentration was found to be unpredictably high and low variable in plasma, with manifest individual differences. Hence, it is very essential to monitor the concentration of 6-MP.[28]

Numerous approaches have been devoted for the detection of 6-MP in biological preparation and pharmaceutical comprising capillary electrophoresis,[29] high-performance liquid chromatography,[30] laser-induced fluorescence,[31] spectrofluorimetry,[32] and chemiluminescence.[33] However, these methods require tedious experimentation. Electrochemical approaches have shown notable advantages in the investigation of drugs in human urine and pharmaceutical preparations. These methods in pharmaceutical analysis are studied owing to their accuracy and precision, low cost, simplicity and rapidity, sensitivity.

In this research work, the voltammetric method have been applied to depict the electrochemical nature of 6-MP on the carbon paste electrode (CPE) in the presence of highly electroactive AHMT-Ag NCCP as a suitable nanosensor in phosphate buffer (pH 7). Further, the developed sensor was also effectively explored to assay 6-mercaptopurine (6-MP) in real samples of blood serum, urine and tablet.

2. RESULTS AND DISCUSSION

The coordination polymer AHMT-Ag is a remarkably symmetrical architecture which provides coordination position for bonding and construct a well-predictable network with various interactions and unique capacity to frame π stacking all over aromatic array. Here, sulfur and nitrogen atoms of AHMT coordinated with Ag(I) into a huge array of polymeric chain. The synthesized AHMT-Ag was characterized by UV−visible spectroscopy, X-ray photoelectron spectroscopy (XPS), Fourier transform infrared spectroscopy (FT-IR), X-ray diffraction (XRD), ^{1}H NMR, high-resolution transmission electron microscopy (HR-TEM), high-resolution scanning electron microscope (HR-SEM), energy-dispersive system (EDS) mapping, energy dispersive X-ray (EDX), and thermal study.

2.1. Materials Characterizations. The FT-IR spectrum of AHMT shows various bands in the region 3270−2930 because of ν(N−H) and ν(NH_2). The peak broadness recommends intramolecular hydrogen bonding (Figure 1I). The vibrational band at 3209 cm^{-1} is initiated because of ν(NH−NH_2) of AHMT and remarkably attenuated to 3095 cm^{-1} in AHMT-Ag, spotting the connection of the exocyclic NH−NH_2 with Ag. Additionally, the S−H stretching of AHMT evidenced at 2789 cm^{-1}disappeared in AHMT-Ag; which indicates thiol ionization, bonding of sulfur via the silver atom. The thioamide band I at 1501 cm^{-1} in AHMT appeared at a higher wave number 1633 cm^{-1} in AHMT-Ag caused by a decrease in the major contributor ν(N−H), and a substantial increase in the minor contributor ν(C═N), respectively, because of sulfur and silver bonding. Furthermore, typical thioamide band II 1315−1346 cm^{-1} in AHMT with the significant contributor ν(C═N) increased considerably to 1365 cm^{-1} in AHMT-Ag, encouraging the bonding of silver with sulfur.

Further XRD was executed in order to investigate the crystal structure. The XRD of AHMT-Ag and AHMT were correlated with Ag(0) attained from the JCPDS file (CAS number 87-0720). AHMT-Ag displays the crystalline nature as shown in S2 Figure S2. It is noticeable that structural characteristics of AHMT and Ag(0) are absent in AHMT-Ag. The crystallographic phase of AHMT-Ag, NCCP was examined at room temperature by XRD with a diffraction angle between 5° and 80°. The, DICVOL04.51 (auto-indexing program) was employed to index the XRD pattern of AHMT-Ag.[34] It was found that experimental diffraction peaks could be indexed using monoclinic, orthorhombic, and triclinic cells. In order to determine the correct crystallographic symmetry for the observed XRD spectra, AHMT-Ag was investigated by Le-Bail refinement through FullProf[35] for different probable crystal structures; for example, orthorhombic *Pnma*, monoclinic $P2_1/m$, *Pm*, and triclinic P1 space groups. It shows that the triclinic crystal structure has the closest fit between the calculated and experimentally observed profiles of AHMT-Ag with a good figure of merit, and it indexed all the diffraction peaks. Figure 1II reveals the experimentally observed data point which are indicated with dotted red circles, while the calculated pattern is shown as a continuous solid line and the variation of the observed from calculated pattern is shown by

DOI: 10.1021/acsomega.9b01122
ACS Omega 2019, 4, 16733−16742

the continuous bottom green line obtained by the Le-Bail fit for space group "triclinic P1". The vertical lines indicate the Bragg peak locations in the difference plot. From Figure 1II it can be clearly observed that the diffraction peaks emerge in the pattern representing a good crystalline nature of synthesized AHMT-Ag NCCP. The triclinic cell has the lattice parameters a = 11.055(1), b = 4.4964(1), c = 5.6471 (2), α = 91.62(4), β = 93.34(1), and γ = 90.28(2) and a unit cell volume 280.30(1) A^3. The crystallinity of AHMT-Ag is again examined by selected area diffraction of transmission electron microscopy (TEM). The diffraction peaks of AHMT-Ag are indexed. The absorption spectra difference shows the interaction effect of metal (S3 Figure S3). AHMT has remarkable a absorbance at 360 nm, and the fellow AHMT-Ag reveals a characteristic absorbance at 270 nm. Signature of hypsochromic shift in the absorbance spectra is because the interaction between AHMT and Ag. XPS enlightens the chemical environment of the elements in AHMT-Ag and the oxidation state of the Ag center. The fitted peaks using software, XPS peak 4.1 (Figure 2) imparts two doublets fitted for Ag (3d). The specific peak at

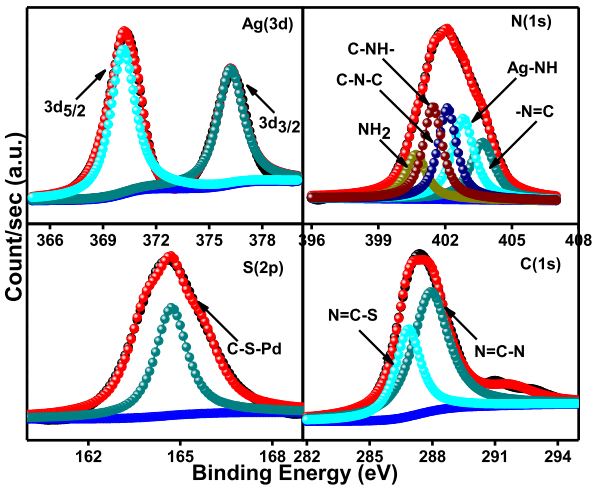

Figure 2. XPS spectra of AHMT-Ag for Ag (3d), N (1s), S (2p), and C (1s) regions.

376.2 eV is the centered feature peak of the $3d_{3/2}$ Ag(I),[36] meanwhile the peak at 370.4 eV is the signature of the $3d_{5/2}$ Ag(I) supporting the oxidation state of silver. N (1s) peaks deliver 5 sets of the singlet in which the peak at 403.7 eV corresponds to the binding energy of endocyclic amine nitrogen (=N−). Binding energy of 402.7 eV attributed to −NH groups, superior binding energy acquainted to the bonding of silver with nitrogen of −NH. Additionally binding energy at 400.6, 402.1, and 401.4 eV correspond to nitrogen of $-NH_2$, C−N−C, and C−NH−[37,38] The binding energy at 164.6 eV appears because of sulfur ($2p_{3/2}$). A variation of binding energy favors coordination of the silver atom with exocyclic sulfur. Binding energy at 287.8 and 286.8 eV denotes that the C (1s) spectrum for the suitable fit analogous to N=C−N− and −N=C−S− bonding.[39]

The ^{1}H NMR spectrum of AHMT has signals at 12.8 that have significance for the ring NH, 7.13 for NH of the $NHNH_2$, 5.4 for SH, and 5.264 ppm for NH_2 of the $NHNH_2$ protons relative to TMS. The absence of signal because the SH proton in AHMT-Ag NCCP establishes the bonding of silver through sulfur. The peak that appeared at 4.10 ppm is because of the NH_2 of NNH_2 in AHMT-Ag. The peak of $NHNH_2$ and NH observed at a lower field, that is, 5.265 and 7.135 ppm, respectively, in AHMT-Ag furnishes bonding of silver with the $NHNH_2$ group of AHMT. The signal corresponding to the S=C−NH proton at 8.406 diminishes in AHMT-Ag NCCP which may be because of bonding of the metal with the sulfur atom of C−S. The doublet at 5.438 also vanished in AHMT-Ag assigning interaction of the metal with the NH_2 group of $NH-NH_2$. The signal corresponding to $N-NH_2$ remained in AHMT-Ag emphasizes the unreacted proton of the amino group (S4 Figure S4).

The morphology and elemental investigation of AHMT-Ag, explored by the HR-TEM, HR-SEM, and SAED pattern shown in Figure 4 provokes a crystalline nanoglobular shaped network

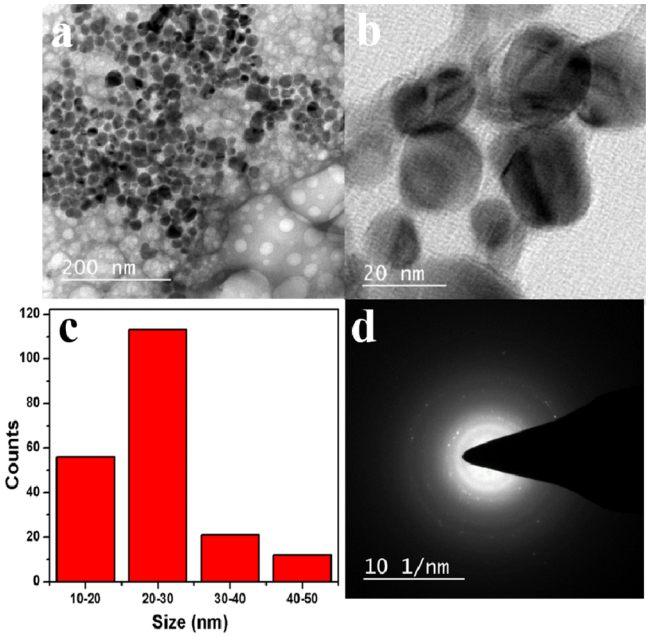

Figure 4. HR TEM of AHMT-Ag (a,b), size distribution graph from the TEM image (c) and corresponding the SAED pattern (d).

structure (S5 Figure S5). The average particle size distribution of AHMT-Ag NCCP was analyzed with Image J software and it shows an average size 20−30 nm (Figure 4c). The irregular nanoglobules profile of the distinct AHMT-Ag was also

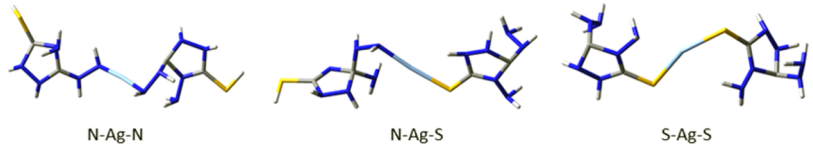

Figure 3. Three possible structures of the AHMT dimer coordinated with the Ag atom obtained at the B3LYP/6-31G**+LanL2DZ level of theory in water solvent.

DOI: 10.1021/acsomega.9b01122
ACS Omega 2019, 4, 16733−16742

captured in the HR-TEM micrograph Figure 4a,b. The SAED pattern illustrates the crystalline nature of the AHMT-Ag network (Figure 4d). The corresponding EDX measurements reveals the elemental composition of AHMT-Ag and verifies the presence of S,N, C, and Ag atoms in the selected area as presented in S6 Figure S6. The EDS mapping illustrate the elemental composition of AHMT-Ag. Here, the overlap image discloses homogeneous distribution of Ag, C, N, and S signifying the formation of the dense polymeric chain. The consequent images (S7 Figure. S7) reveal the mapping of discrete elements and evidences the higher nitrogen concentration.

Moreover, the molecular modeling is implemented to achieve the favored orientation of the ligand in the network which certifies antialignment, the favored orientation. (S8 Figure S8)

Furthermore, there could be three possible ways for coordination of Ag with ligand 4-amino-3-hydrazino-5-mercapto-1,2,4,-triazole (AHMT). Density functional theory (DFT) study was executed in order to assess the most probable way of interaction. Two ligand units were under investigation with the metal. Geometries of all the dimers were optimized in a water solvent using the B3LYP[40] functional and LanL2DZ basis set for the Ag atom and the 6−31g** basis set for the rest of the atoms. The genuineness of the calculated structures was confirmed by visually examining the vibrational modes related to all real vibration frequencies. All the calculations were accomplished by the Gaussian[41] program and GaussView program was used for visualization of optimized structures and vibrational modes. A most appropriate structure has been proposed after the coordination of Ag with AHMT. Three possible structural considerations were optimized using DFT (Figure 3). Gibbs free energies of all the three structures of the Ag-coordinated AHMT dimer were obtained at the B3LYP/6-31G**+LanL2DZ level of theory in the water solvent. The N−Ag−S structure was more stable than N−Ag−N and S−Ag−S by 1.44 and 4.62 eV, respectively.

Based on these findings the structure of nanocrystalline AHMT-Ag is proposed (Figure 5). Ag(I) centers are linked

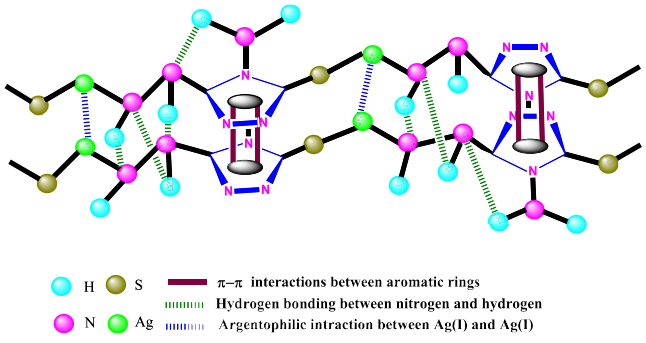

Figure 5. Proposed structural network of AHMT-Ag.

with coordination sites of AHMT via sulfur and nitrogen atoms throughout the arrangement and adjacent layers are stabilized through π stacking of the aromatic ring and the intermolecular hydrogen bonding.

In order to investigate stability of the coordination network, zeta potential of prepared NCCP was measured by using the dynamic light scattering instrument. The charge on NCCP plays an important role in accumulation. Larger positive or negative charge repels each other and prevents accumulation. Zeta potential at −49 mV shows the extensively stable network of NCCP (S9 Figure S9).

Further, thermo-gravimetric properties of AHMT-Ag are studied under a nitrogen environment for analysis of the thermal stability and thermal decomposition activation energy. The thermal decomposition of AHMT and AHMT-Ag was illustrated by the thermal-gravimetric curve TGA (S10 Figure S10). AHMT-Ag shows a significant weight loss revealing thermally stable till 222 °C disclosing a thermally strong network of the coordination polymer. AHMT-Ag displays first degradation at a lower temperature than AHMT which explores the presence of the coordination linkage in AHMT-Ag. Here, first decomposition at 222 °C corresponds to the rupture of the coordination linkage. The minor degradation detected at 100 °C is due to uncoordinated water molecules in both AHMT and AHMT-Ag. Further, consecutive degradation in the TGA plot is due to the thermal breakdown of byproducts and is the same in both AHMT and AHMT-Ag.[42] Activation energy of AHMT-Ag related to thermal degradation is determined via the Broido equation[43] to be 11.39 kJ/mol (S11 Figure S11).

2.2. Electro Activity of AHMT-Ag. *2.2.1. Electrode Active Surface Area.* Electroactivity of the AHMT-Ag NCCP-modified CPE surface is probed by an Fe(III)/Fe(II) redox system and the unmodified CPE, AHMT-Ag/CPE active surface area are calculated to be 0.03 and 0.14 cm^2. These reveal a substantial rise in the AHMT-Ag/CPE effective surface area by a factor of 4 caused by larger exposure and density in the nanoarchitecture modified electrode. (S12 Figure S12)

2.3. Electrochemical Detection of 6-MP. The remarkably efficient electroactivity of AHMT-Ag/CPE has been employed to quantify the immunosuppressive drug 6-MP in various media and for this, the reaction condition was monitored and optimized.

2.3.1. Optimization of Reaction Conditions. 2.3.1.1. Effect of pH. Effect of pH on electrochemical detection of 6-MP was studied and the results are shown in S13 Figure S13. It shows that as pH increases the anodic potential displays a negative shift which leads to deprotonation before electron transfer in the electro-oxidation mechanism and is an obvious behavior of biological sulphydryl compounds.[44,45] The anodic current increases up to pH 7 and then decreases therefore, pH 7 is selected as optimum for 6-MP oxidation. The pH of the buffer was optimized to 7 for the whole quantification spectrum of the drug.

2.3.1.2. Effect of the Scan Rate. The plot of i_p (anodic current) versus $\nu^{1/2}$(square root of the scan rate) displays the diffusion-controlled mechanism of 6-MP electro-oxidation on AHMT-Ag/CPE and explores adsorption on the surface of the electroactive electrode (S14 Figure S14b).

2.3.1.3. Number of Electrons Transferred (n_a). The electrons involved in the electro-oxidation of 6-MP (n_a) is calculated to be 1.64 using the Laviron equation (S14, Figure S14a,c) and ensures that irreversible oxidation of 6-MP is a two electron procedure at AHMT-Ag/CPE, followed by the previous report.[46,47]

2.3.1.4. Effect of Matrix. Effect of matrix is the collective effect of several ingredient of the sample other than the analyte during quantitative analysis. It reduces or increases the analyte response. Dilution with solvent is the best approach to suppress the matrix effects. Therefore, mixed blank serum and phosphate-buffered saline (PBS) (pH 7.0) were both spiked

DOI: 10.1021/acsomega.9b01122
ACS Omega 2019, 4, 16733−16742

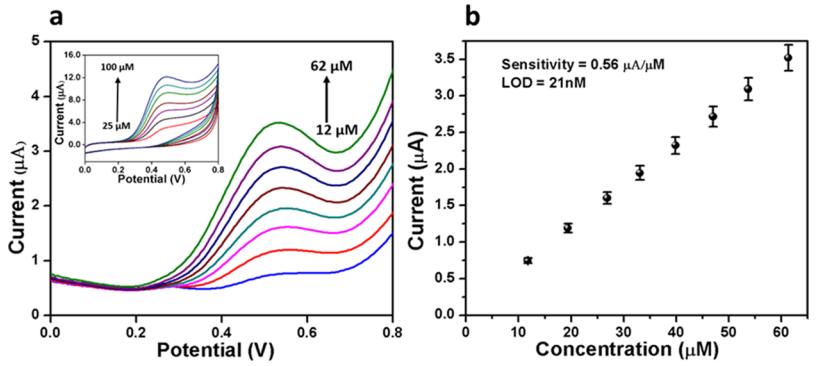

Figure 6. (a) Differential pulse voltammogram recorded on AHMT-Ag/CPE in 0.1 M PBS (pH 7) by successive addition of 6-MP, the inset of (a) cyclic voltammogram recorded by successive addition of 6-MP, (b) corresponding calibration plot.

Scheme 1. Possible Mechanism for Formation of AHMT-Ag

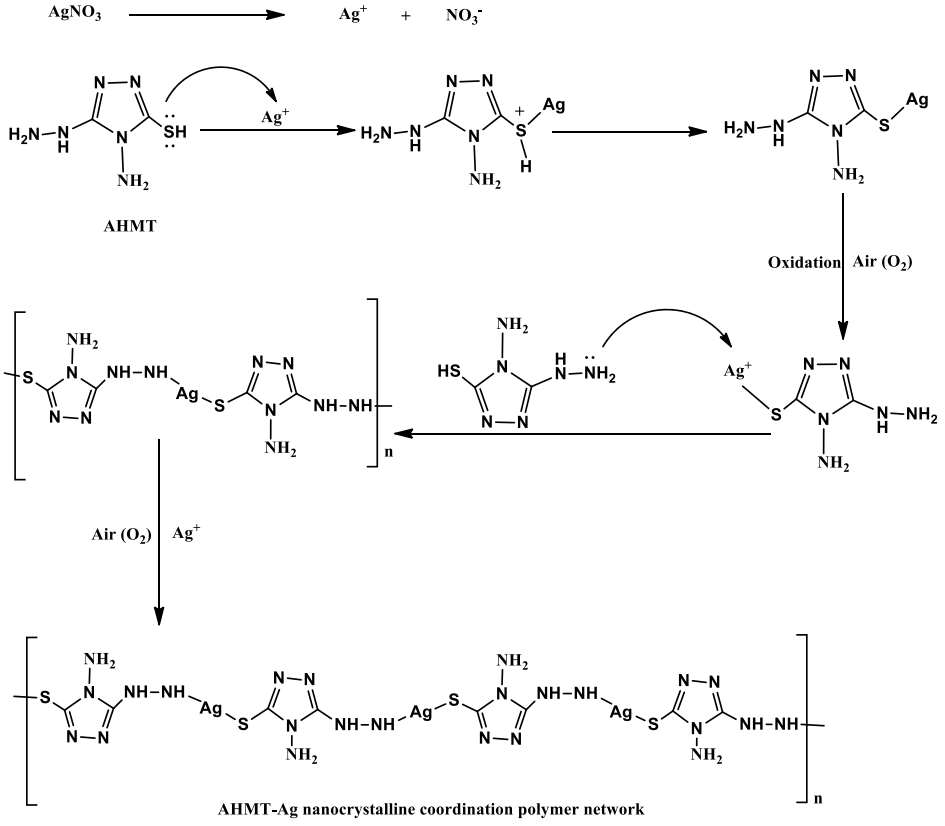

with 6-MP (60 μM), diluted with PBS (pH 7.0) at 20, 50, 100, 120, and 150-fold, and analyzed, respectively, to explore the matrix effect. At 20-fold dilution, the serum discloses lower anodic peak current and higher anodic peak potential than PBS (Figure S15A,B). Increasing the dilution, the peak current remains stable and the anodic peak potential reduces from 50 to 100-fold in serum. Contrary, the peak current diminishes sharply while the peak potential rises slightly in PBS. For 100-fold onward dilution, anodic peak current and potential have almost constant values. These outcomes demonstrate the 100 times dilution which evidences the elimination of the matrix effect of serum and guarantees the high sensitivity and thus adopted for the consequent analysis.

The electroactivity of AHMT-Ag/CPE was explored for the thorough and broad spectrum voltammetric assay of 6-MP in PBS at optimized pH 7.0. A featured anodic signature exhibits at 0.48 V in the voltammogram of cyclic voltammetry (CV) and differential pulse voltammetric (DPV) using AHMT-Ag/CPE is a crucial signature of 6-MP electro-oxidation. In order to establish the complete experimentation, the plot for the consecutive addition was observed (Figure 6) which shows anodic peak enhancement with the successive addition in both CV and DPV. The calibration graph for DPV, executes linear dependency of anodic current with drug concentration and provides the limit of detection as 21 nM and sensitivity 0.56 μA/μM with the regression value of 0.99 at the S/N ratio (signal/noise): 3.

The anodic peak increases significantly with the sequential addition of drug because the AHMT-Ag modified electrode endorsed the electro-oxidation of 6-MP. Here 6-MP approaches to the modified electrode and gets attached. The driving force for the endorsement of attachment and electro-

DOI: 10.1021/acsomega.9b01122
ACS Omega 2019, 4, 16733−16742

oxidation is (a) intermolecular hydrogen bonding between amino groups, (b) the effective electron channeling of AHMT-Ag which assist the faster electron transfer through the electrode, (c) the $\pi-\pi$ electron coupling of aromatic rings, (d) hydrophobic interaction between duplex AHMT-Ag and 6-MP, (e) high surface area of AHMT-Ag, and (f) electro-catalytic efficiency of Ag promote the electro-oxidation of 6-MP. The schematics for electro-oxidation of 6-MP at the AHMT-Ag platform is presented, it occurs through transfer of two electrons and two protons and electron channeling occurs through the AHMT-Ag platform (Scheme 2).

Scheme 2. Mechanism for Electro-Oxidation of 6-MP

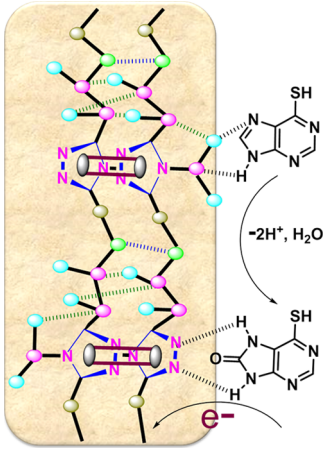

In order to verify the broad spectrum applicability of the sensor, AHMT-Ag/CPE was used to assay 6-MP in pharmaceutical formulation of the drug. The sample solution was developed in buffer and pH was maintained at 7. This spiked solution of the tablet was utilized for the voltammetric assay under the same experimental conditions optimized for the ideal situation using both CV and DPV and shown in Figure 7. The CV and DPV response for the successive addition of the drug exhibit an anodic peak at 0.48 V with corresponding to 6-MP oxidation. The corresponding calibration plot for the detection shows a linear response of anodic current with a concentration of 6-MP up to 120 μM with a limit of detection 37 nM and a regression value 98% validating the sensing approach in clinical formulation.

2.4. Validation of Method. Various constituents present in serum and urine coexist; therefore, the primary objective of this report was to assess and explore the ability of the sensor to assay 6-MP in urine and serum. The urine and serum samples were diluted and buffered to pH 7. The developed sensor explores the dependence of an anodic peak current of 6-MP on concentration. The plot for consecutive addition is displayed (Figures 8 and 9) which provides a limit of detection 97 and 87 nM , respectively, using DPV results. The sensitivity diminished in urine and serum which may be because of the matrix effect. In the light of these results, the developed sensing platform is highly sensitive and versatile for detection of 6-MP which is authenticated in clinical formulation, human urine as well as serum samples. The characteristic envisioned anodic current event is figured at 0.48 V. Further, the proposed method was compared with various reported methods for 6-MP detection through a bar diagram (Table S2 and Figure S17). The proposed system provides the least detection limit among the existing literature for 6-MP assay and thus supports the better efficiency of the designed sensor.

The serum sample was investigated by the electrochemical assay. Pearson's correlation analysis discloses a substantial relationship of 6-MP concentrations in serum analyzed by the electrochemical method (r = 0.9131, 0 < p < 1) (Figure 9).

The matrix effect of serum has been studied with direct dilution and avoided the complex modification process. The sensitivity of the method was significant covering fairly low and lethal 6-MP concentrations. This encouraging work is to develop a simple, accurate, and practical electrochemical method for the determination of 6-MP in plasma for clinical diagnosis.

2.5. Interference and Repeatability Test. Interference study was performed to examine the specificity of the electrochemical sensor by using 6-MP (55 μM) with and without 100 μM solution of interfering substances through the designed electrochemical technique (Figure 10). It can be noticed that the electrochemical current response deviation due to the interfering agent was <5% of without interferences, representing excellent selectivity of designed electrochemical sensors. Further, the reproducibility was confirmed by performing the repeatability test in both interday (1, 2, 3, and 4 days) and intraday (0, 2, 4, and 6 h). Figure S16a,b shows intra and interday repeatability test by differential pulse voltammogram at the fixed potential 0.48 V recorded on AHMT-Ag/CPE in 0.1 M PBS (pH 7) by successive addition of 6-MP.

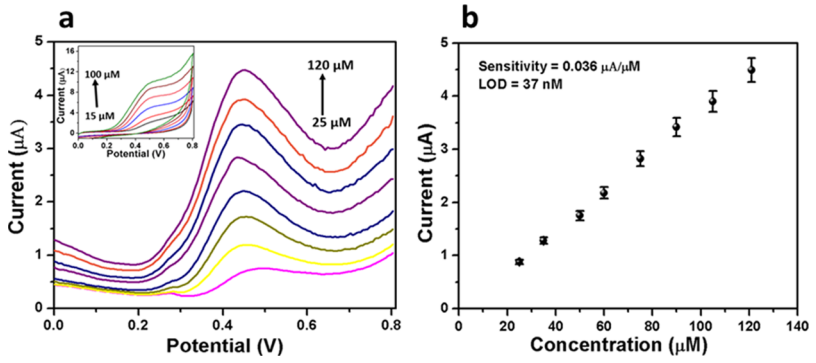

Figure 7. (a) Differential pulse voltammogram recorded on AHMT-Ag/CPE in 0.1 M PBS (pH 7) by successive addition of the 6-MP tablet, the inset of (a) cyclic voltammogram recorded by successive addition of 6-MP, (b) corresponding calibration plot.

DOI: 10.1021/acsomega.9b01122
ACS Omega 2019, 4, 16733−16742

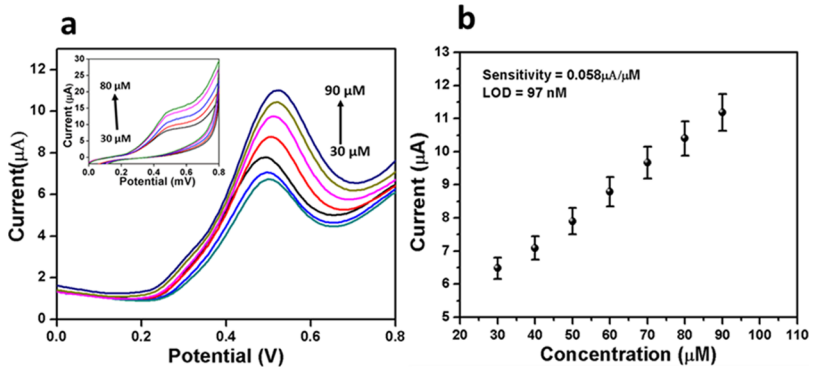

Figure 8. (a) Differential pulse voltammogram recorded on AHMT-Ag/CPE in the urine sample by successive addition of 6-MP, the inset of (a) cyclic voltammogram recorded by successive addition of 6-MP, (b) corresponding calibration plot.

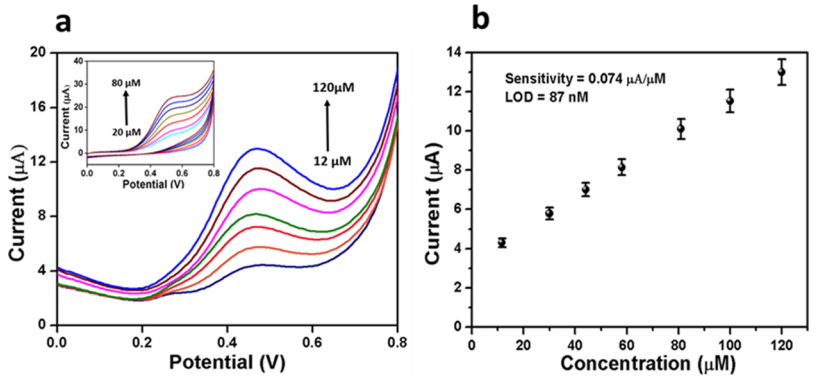

Figure 9. (a) Differential pulse voltammogram recorded on AHMT-Ag/CPE in the serum sample by successive addition of 6-MP, the inset of (a) cyclic voltammogram recorded by successive addition of 6-MP, (b) corresponding calibration plot.

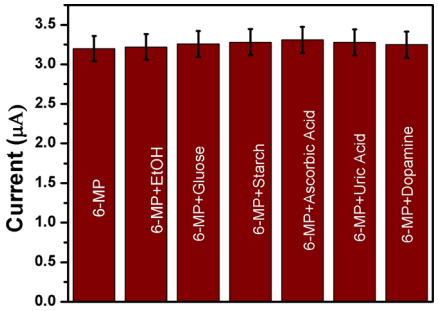

Figure 10. DPV responses of the electrochemical sensor to 55 μM 6-MP, 55 μM 6-MP+ 100 μM ethanol, 55 μM 6-MP + 100 μM glucose, 55 μM 6-MP+ 100 μM starch, 55 μM 6-MP+ 100 μM ascorbic acid, 55 μM 6-MP+ 100 μM uric acid, and 55 μM 6-MP+ 100 μM dopamine. Error bar = RSD, (n = 5).

3. CONCLUSIONS

This article provides the development of an elegant nanocrystalline polymeric network of AHMT-Ag which provides a geometrically and symmetrically feasible highly sensitive platform for the ultra-trace and whole spectrum systematic and potential quantification of 6-MP. The effective electron channeling through the nanocrystalline architecture is essential for facile production of feature-centered events. The complete experimentation depicted that serendipitous use of AHMT-Ag is crucial for generating distinctive current patterns in characteristic events. This feature endows high confidence assay at an ultratrace level. The key of success of the sensing methodology is the feasible and faster electron channeling through the nanocrystalline polymeric platform. The potential of the study is enzymeless, cost-effective, and complete spectrum ultratrace detection of 6-MP. This strategy can be explored in the commercial portable device fabrication for a variety of anticancer drugs.

4. EXPERIMENTAL SECTION

4.1. Chemicals and Materials. AHMT was purchased from Sigma-Aldrich USA. Silver salt ($AgNO_3$), 6-MP monohydrate (6-MP), TEMPO, sodium hydroxide, and BHT were bought from SRL chemical (India) and used as accepted unless mentioned otherwise. Aqua regia was used for cleaning of the glassware, after rinsing with the mixture of ultrapure water and ethanol, Merck India. 6-MP solution was freshly equipped by using doubly deionized water and ethanol mixture solution (1:1). The electrodes used to prepare the carbon-paste electrode were procured from bio-analytical organization. Human urine and blood serum samples were obtained from authorized hospitals. The tablet of 6-MP was acquired through a local supplier (Cipla Ltd. India); reaction solutions were exposed in pure nitrogen to remove oxygen and avoid any external oxidation during each electrochemical measurement.

4.2. Electrode Fabrication. 1 mm diameter CPE used for modification was obtained from BASi (Indiana). Carbon paste was prepared by mixing 67% w/w graphite powder, 2.5% w/w paraffin oil, and 35% w/w AHMT-Ag then the cavity of the electrode was filled with a portion of the resulting paste. The surface of the CPE was smoothed against butter paper and

DOI: 10.1021/acsomega.9b01122
ACS Omega 2019, 4, 16733−16742

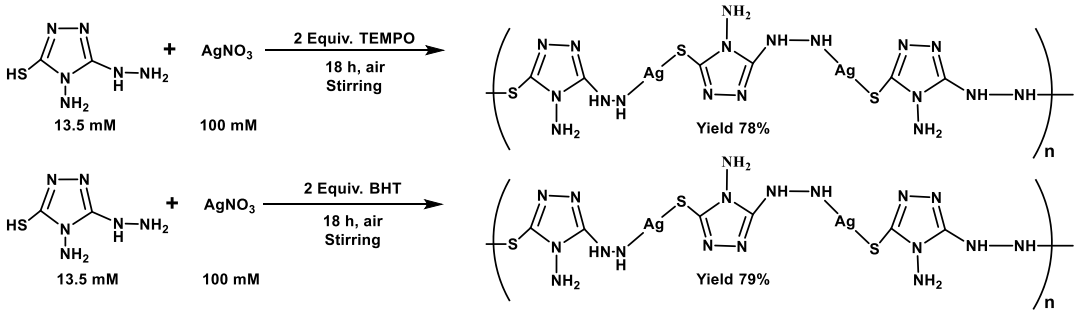

Figure 11. Schematic illustration of controlled experiments for the formation of AHMT-Ag using TEMPO and BHT.

rinsed with distilled water. The carbon paste was cautiously removed prior to pressing a new fraction into the electrode after each measurement.

4.3. Instrumentation. The PerkinElmer 783 spectrometer was used to record FT-IR spectra of AHMT-Ag and AHMT in the range of 3600−500 cm^{-1} on a KBr disc. Powder XRD were executed in the range of 5°−80° by using a Miniflex 600 diffractometer with Cu Kα radiation (Kα = 1.54056 Å) with a 2°/min scan rate. UV−vis was performed in a quartz cuvette (1 cm path length) by using a Biotech, Epoch 2 microplate reader spectrophotometer, USA. For elemental analysis XPS (X-ray photoelectron spectrometry) was executed with, Shimadzu Group Company, Kratos analytical instrument, XPS (UK), with 1.254 Å Mg Kα radiations. Nova, Nano-SEM 450 FEI (Netherlands) was used for the recording HR-SEM. An FEI TECHNAI G^2 20 TWIN Czech Republic electron microscope was used for recording HR-TEM, EDS mapping, and EDX with 200 keV (accelerating voltage) on a copper grid (carbon-coated) prepared by 6 μL of polymer solution. A Mettler Toledo TGA/DSC 1 STARE System, Switzerland was used for thermal analysis. TGA and DTA were performed in an inert atmosphere with a heating rate of 10 °C min^{-1}. All electrochemical measurements were accomplished on a Ω Metrohm, 797 VA, Computrace trace analyzer, Switzerland, using a three electrode assembly by electrochemical software 3.1 with AHMT-Ag-modified CPE (working electrode), Pt foil (counter electrode), Ag/AgCl (reference electrode), and pH 7.0 phosphate buffer used as supporting electrolytes for all electrochemical measurements.

4.4. Experimental Procedure for AHMT-Ag Synthesis. 13.5 mM aqueous/ethanolic solution of AHMT and 100 mM ethanolic solution of $AgNO_3$ were prepared. Further, the $AgNO_3$ solution was dropwise added in the AHMT solution with continuous stirring for 24 h at atmospheric pressure and room temperature. A blackish-grey precipitate of AHMT-Ag NCCP was obtained then the obtained precipitate was washed three times after filtration followed by water−ethanol mixture solution (1:1 v/v %) to remove the unreacted AHMT and $AgNO_3$. Removal of the solvent was regulated at 40 °C in vacuum and the obtained yield was 87%. (S1 Figure S1)

4.5. Radical Controlled Experiments. The radical-controlled experiments with BHT (2,6-di-*t*-butyl-4-hydroxytoluene) and TEMPO (2,2,6,6-tetramethyl-1-piperidinyl oxidanyl) trapping agents, endows the cationic pathway without any interference under standard conditions (Figure 11). Mechanism involves silver ions as a cationic companion for initiating polymerization and launching the silver-associated monomeric segment which activates Ag oxidation to furnish AHMT-Ag.[47] (Scheme 1). Thereafter structural and bonding information is reviewed under FT-IR, ^{1}H NMR, and XPS analysis.

■ ASSOCIATED CONTENT

Supporting Information

The Supporting Information is available free of charge on the ACS Publications website at DOI: 10.1021/acsomega.9b01122.

The synthesis of AHMT−Ag, comparative study of XRD of AHMT−Ag with AHMT and Ag(0), UV−vis spectra of AHMT and AHMT-Ag, ^{1}H NMR of AHMT and AHMT-Ag, HR SEM of AHMT-Ag, energy-dispersive X-ray spectroscopy, EDS mapping, molecular mechanics calculation, molecular mechanics calculation, zeta potential graph of AHMT-Ag, thermogravimetric analysis, the activation energy for thermal decomposition, the CV of the electrodes in 5 mM Fe(III) in PBS pH 7, effect of the scan rate, the CV micrograph at various pH, effect of matrix, repeatability test, the analytical superiority of the present work, and comparison of various systems for detection of 6-MP (PDF)

■ AUTHOR INFORMATION

Corresponding Author

*E-mail: rprakash.mst@iitbhu.ac.in.

ORCID

Akhilesh Kumar Singh: 0000-0001-8729-7318

Rajiv Prakash: 0000-0002-6623-522X

Notes

The authors declare no competing financial interest.

■ ACKNOWLEDGMENTS

The authors are thankful to CIF IIT (BHU) for providing the instrumentation facility. The first author acknowledges the Department of Chemistry, Deen Dayal Upadhyaya Gorakhpur University, Gorakhpur, India. The authors do not have any conflict of interest.

■ REFERENCES

(1) Rodpun, K.; Lucas, N. T.; Tan, E. W.; Meledandri, C. J. Development of Solvent-Dispersible Coordination Polymer Nanocrystals and Application as Efficient Heterogeneous Catalysts. *Cryst. Growth Des.* **2016**, *16*, 3940−3946.

(2) Pan, L.; Sander, M. B.; Huang, X.; Li, J.; Smith, M.; Bittner, E.; Bockrath, B.; Johnson, J. K. Microporous Metal Organic Materials: Promising Candidates as Sorbents for Hydrogen Storage. *J. Am. Chem. Soc.* **2004**, *126*, 1308−1309.

(3) Rowsell, J. L. C.; Yaghi, O. M. Metal−organic frameworks: a new class of porous materials. *Microporous Mesoporous Mater.* **2004**, *73*, 3−14.

DOI: 10.1021/acsomega.9b01122
ACS Omega 2019, 4, 16733−16742

(4) Gupta, B.; Prakash, R. Interfacial polymerization of carbazole: Morphology controlled synthesis. *Synth. Met.* **2010**, *160*, 523−528.
(5) Xu, X.; Lu, Y.; Yang, Y.; Nosheen, F.; Wang, X. Tuning the growth of metal-organic framework nanocrystals by using polyoxometalates as coordination modulators. *Sci. China Mater.* **2015**, *58*, 370−377.
(6) Tiwari, M.; Kumar, A.; Shankar, U.; Prakash, R. The nanocrystalline coordination polymer of AMT−Ag for an effective detection of ciprofloxacin hydrochloride in pharmaceutical formulation and biological fluid. *Biosens. Bioelectron.* **2016**, *85*, 529−535.
(7) Vinita; Vinita, N. R.; Prakash, R. One step synthesis of AuNPs@ MoS2-QDs composite as a robust peroxidase- mimetic for instant unaided eye detection of glucose in serum, saliva and tear. *Sens. Actuators, B* **2018**, *263*, 109−119.
(8) Ren, C.; Liu, P.; Wang, Y. Y.; Huang, W.-H.; Shi, Q. Z. Structural Investigation of Coordination Polymers Constructed from a Conformational Bis-triazole Ligand and V-Shaped Bridging, Carboxylate Anions: Hydrothermal Syntheses, Crystal Structures, and Property Studies. *Eur. J. Inorg. Chem.* **2010**, 5545−5555.
(9) Melvin, A.; Vijay, R.; Chaudhari, V.-R.; Gupta, B.; Prakash, R.; Haram, S.; Baskar, G.; Khushalani, D. A facile methodology for the design of functionalized hollow silica spheres. *J. Colloid Interface Sci.* **2010**, *346*, 265−269.
(10) Cho, W.; Lee, H. J.; Choi, S.; Kim, Y.; Oh, M. Highly effective heterogeneous chemosensors of luminescent silica@coordination polymer core-shell micro-structures for metal ion sensing. *Sci. Rep.* **2015**, *4*, 6518.
(11) Tiwari, M.; Kumar, A.; Prakash, R. Nano-porous network of DMTD-Ag coordination polymer for the ultra trace detection of anticholinergic drug. *Polymer* **2016**, *82*, 66−74.
(12) Jambovane, S. R.; Nune, S. K.; Kelly, R. T.; McGrail, B. P.; Wang, Z.; Nandasiri, M. I.; Katipamula, S.; Trader, C.; Schaef, H. T. Continuous, One-pot Synthesis and Post-Synthetic Modification of NanoMOFs Using Droplet Nanoreactors. *Sci. Rep.* **2016**, *6*, 36657.
(13) Lee, J.; Farha, O. K.; Roberts, J.; Scheidt, K. A.; Nguyen, S. T.; Hupp, J. T. Metal−organic framework materials as catalysts. *Chem. Soc. Rev.* **2009**, *38*, 1450.
(14) Vinita; Nirala, N. R.; Tiwari, M.; Prakash, R. A nanoporous palladium(II) bridged coordination polymer acting as a peroxidase mimic in a method for visual detection of glucose in tear and saliva. *Microchim. Acta* **2018**, *185*, 245.
(15) Furukawa, H.; Miller, M. A.; Yaghi, O. M.; Heuchel, M.; Harting, P.; Quitzsch, K.; Jaroniec, M.; Gameson, I.; Anderson, P.-A.; Harris, I.-R. Independent verification of the saturation hydrogen uptake in MOF-177 and establishment of a benchmark for hydrogen adsorption in metal−organic frameworks. *J. Mater. Chem.* **2007**, *17*, 3197.
(16) Rieter, W. J.; Taylor, K. M. L.; An, H.; Lin, W.; Lin, W. Nanoscale Metal−Organic Frameworks as Potential Multimodal Contrast Enhancing Agents. *J. Am. Chem. Soc.* **2006**, *128*, 9024−9025.
(17) Cohen, S. M. Modifying MOFs: new chemistry, new materials. *Chem. Sci.* **2010**, *1*, 32−36.
(18) Jambovane, S. R.; Nune, S. K.; Kelly, R. T.; McGrail, B. P.; Wang, Z.; Nandasiri, M. I.; Katipamula, S.; Trader, C.; Schaef, H. T. Continuous, One-pot Synthesis and Post-Synthetic Modification of NanoMOFs Using Droplet Nanoreactors. *Sci. Rep.* **2016**, *6*, 36657.
(19) Bétard, A.; Fischer, R. A. Metal−Organic Framework Thin Films: From Fundamentals to Applications. *Chem. Rev.* **2012**, *112*, 1055−1083.
(20) Wang, Y.; Zhang, Y.; Hou, C.; et al. Ultrasensitive electrochemical sensing of dopamine using reduced graphene oxide sheets decorated with p-toluenesulfonate-doped polypyrrole/Fe_3O_4 nanospheres. *Microchim. Acta* **2016**, *183*, 1145.
(21) Jaros, S.-W.; Sokolnicki, J.; Wołoszyn, A.; Haukka, M.; Kirillov, A.-M.; Smoleński, P. A novel 2D coordination network built from hexacopper(i)-iodide clusters and cagelike aminophosphine blocks for reversible "turn-on" sensing of aniline. *J. Mater. Chem. C* **2018**, *6*, 1670−1678.
(22) Lee, C.-Y.; Farha, O.-K.; Hong, B.-J.; Sarjeant, A.-A.; Nguyen, S.-T.; Hupp, J.-T. Light-Harvesting Metal−Organic Frameworks (MOFs): Efficient Strut-to-Strut Energy Transfer in Bodipy and Porphyrin-Based MOFs. *J. Am. Chem. Soc.* **2011**, *133*, 15858−15861.
(23) Xu, X.-Y.; Yan, B. A fluorescent wearable platform for sweat Cl^- analysis and logic smart-device fabrication based on color adjustable lanthanide MOFs. *J. Mater. Chem. C* **2018**, *6*, 1863−1869.
(24) Imaz, I.; Rubio-Martínez, M.; García-Fernández, L.; García, F.; Ruiz-Molina, D.; Hernando, J.; Puntes, V.; Maspoch, D.; Muderspach, L.; Garcia, A.; Burnett, A.; Greco, F.-A.; Morrow, C.-P.; Paradiso, L.-J.; Liang, L.-J.; Gil, S.; Férey, G.; Couvreur, P.; Gref, R. Coordination polymer particles as potential drug delivery systems. *Chem. Commun.* **2010**, *46*, 4737.
(25) Nirala, N. R.; Vinita; Prakash, R. Quick colorimetric determination of choline in milk and serum based on the use of MoS2 nanosheets as a highly active enzyme mimetic. *Microchim. Acta* **2018**, *185*, 224.
(26) Inukai, M.; Horike, S.; Itakura, T.; Shinozaki, R.; Ogiwara, N.; Umeyama, D.; Nagarkar, S.; Nishiyama, Y.; Malon, M.; Hayashi, A.; Ohhara, T.; Kiyanagi, R.; Kitagawa, S. Encapsulating mobile proton carriers into structural defects in coordination polymer crystals: high anhydrous proton conduction and fuel cell application. *J. Am. Chem. Soc.* **2016**, *138*, 8505−8511.
(27) Haedler, A. T.; Kreger, K.; Issac, A.; Wittmann, B.; Kivala, M.; Hammer, N.; Köhler, J.; Schmidt, H.-W.; Hildner, R. Long-range energy transport in single supramolecular nanofibres at room temperature. *Nature* **2015**, *523*, 196−199.
(28) Hassan, K.-M.; Abdollah, F.-S.; Khalil, T.; Fatemeh, K.; Shahryar, S.; Reza, M. Simultaneous determination of 6-mercaptopruine, 6-thioguanine and dasatinib as three important anticancer drugs using nanostructure voltammetric sensor employing Pt/MWCNTs and 1-butyl-3- methylimidazolium hexafluoro phosphate. *Biosens. Bioelectron.* **2016**, *86*, 879−884.
(29) Yang, Y.; Zhou, S.; Ouyang, R.; Yang, Y.; Tao, H.; Feng, K.; Zhang, X.; Xiong, F.; Guo, N.; Zong, T.; Cao, P.; Li, Y.; Miao, Y. Improvement in the Anticancer Activity of 6-Mercaptopurine via Combination with Bismuth(III). *Chem. Pharm. Bull.* **2016**, *64*, 1539−1545.
(30) M, E. A.; A, S. M.; Sidhom, I.; Z, M. G.; S, R. H. HPLC Determination of the Levels of 6-Mercaptopurine Metabolites Suitablefor the Clinical Risk Assessment of its Toxicity among Egyptian Children withAcute Lymphocytic Leukemia. *J. Anal. Bioanal. Tech.* **2017**, *8*, 1−11.
(31) Waterval, C. M.; Lingeman, H.; Bult, A.; Underberg, W. J. M. Derivatization trends in capillary electrophoresis. *Electrophoresis* **2000**, *21*, 4029−4045.
(32) Shahrokhian, S.; Ghorbani-Bidkorbeh, F.; Mohammadi, A. Electrochemical capacitive properties of CNT fibers spun from vertically aligned CNT arrays. *J. Solid State Electrochem.* **2012**, *16*, 1643.
(33) Dinarvand, J. P.; Zhang, X. .M. Electrocatalytic Activity of Electropolymerized Cobalt Tetraaminophthalocyanine Film Modified Electrode towards 6-Mercaptopurine and 2-Mercaptobenzimidazole. *S. Afr. J. Chem.* **2010**, *145*, 145−151.
(34) Rodríguez-Carvajal, J. Recent advances in magnetic structure determination by neutron powder diffraction. *Phys. B* **1993**, *192*, 55−69.
(35) Boultif, A.; Louër, D. Indexing of powder diffraction patterns for low-symmetry lattices by the successive dichotomy method. *J. Appl. Crystallogr.* **1991**, *24*, 987−993.
(36) Wang, K.; Wang, H.; Wang, R.; Key, J.; Linkov, V.; Ji, S. Palygorskite Hybridized Carbon Nanocomposite as a High-Performance Electrocatalyst Support for Formic Acid Oxidation. *S. Afr. J. Chem.* **2013**, *66*, 86−91.
(37) Daems, N.; Sheng, X.; Vankelecom, I. F. J.; Pescarmona, P. P. Metal-free doped carbon materials as electrocatalysts for the oxygen reduction reaction. *J. Mater. Chem. A* **2014**, *2*, 4085−4110.
(38) Lee, M.-S.; Park, M.; Kim, H. Y.; Park, S. J.; Zhou, H. C. Effects of Microporosity and Surface Chemistry on Separation Performances

DOI: 10.1021/acsomega.9b01122
ACS Omega 2019, 4, 16733−16742

of N-Containing Pitch-Based Activated Carbons for CO2/N2 Binary Mixture. *Sci. Rep.* **2016**, *6*, 23224.
(39) Lv, M.; Mei, T.; Zhang, C. a.; Wang, X.; Li, X.-Z.; Wei, Y.; Zhang, H.-L.; Yuan, Z.-B.; Jiang, H.-J.; Ma, C.-C.; Hu, C.-C. Selective and sensitive electrochemical detection of dopamine based on water-soluble porphyrin functionalized graphene nanocomposites. *RSC Adv.* **2014**, *4*, 9261.
(40) Lee, C.; Yang, W.; Parr, R. G. Development of the Colle-Salvetti correlation-energy formula into a functional of the electron density. *Phys. Rev. B* **1988**, *37*, 785−789.
(41) Frisch, M.-J.; et al. *Gaussian 09*; Gaussian Inc: Wallingford, CT, USA, 2009, G09/Gaussian.com, http://gaussian.com/glossary/g09/ (accessed 14 March, 2018).
(42) Kaya, İ.; Erçağ, A.; Avcı, A.; Çulhaoğlu, S. Characterization and Conductivity Properties of Novel Oligomer Schiff Bases Derived from 4-Amino-3-hydrazino-5-mercapto-1, 2, 4-triazole and Their Reactions with VO(IV), Cu(II) Ions. *J. Inorg. Organomet. Polym. Mater.* **2014**, *24*, 665−675.
(43) Broido, A. A simple, sensitive graphical method of treating thermogravimetric analysis data. *J. Polym. Sci., Polym. Phys.* **1969**, *7*, 1761−1773.
(44) Shahrokhian, S.; Amiri, M. Voltammetric determination of thiocytosine based on its electrocatalytic oxidation on the surface of carbon-paste electrode modified with cobalt Schiff base complexes. *J. Solid State Electrochem.* **2007**, *11*, 1133−1138.
(45) Shahrokhian, S.; Kamalzadeh, Z.; Bezaatpour, A.; Boghaei, D. M. Differential pulse voltammetric determination of N-acetylcysteine by the electrocatalytic oxidation at the surface of carbon nanotube-paste electrode modified with cobalt salophen complexes. *Sens. Actuators, B* **2008**, *133*, 599−606.
(46) Keyvanfard, M.; Khosravi, V.; Karimi-Maleh, H.; Alizad, K.; Rezaei, B. Voltammetric determination of 6-mercaptopurine using a multiwall carbon nanotubes paste electrode in the presence of isoprenaline as a mediator. *J. Mol. Liq.* **2013**, *177*, 182−189.
(47) Shi, Z.; Zhang, C.; Tang, C.; Jiao, N. Recent advances in transition-metal catalyzed reactions using molecular oxygen as the oxidant. *Chem. Soc. Rev.* **2012**, *41*, 3381.

DOI: 10.1021/acsomega.9b01122
ACS Omega 2019, 4, 16733−16742